Hindawi
International Journal of Photoenergy
Volume 2020, Article ID 8868782, 7 pages
https://doi.org/10.1155/2020/8868782

Research Article

Microstructure Optimization of Mos_2/Sepiolite Nanocomposites via a Surfactant-Assisted Hydrothermal Strategy for High Efficiency Photocatalysis

Li Cui,[1,2] Ming Hao,[1,2] Fei Wang,[1,2] Baizeng Fang,[3] Jinsheng Liang,[1,2] Maomao Zhu,[1,2] and Xinlei Xie[1,2]

[1]*Key Laboratory of Special Functional Materials for Ecological Environment and Information (Hebei University of Technology), Ministry of Education, Tianjin 300130, China*
[2]*Institute of Power Source and Ecomaterials Science, Hebei University of Technology, Tianjin 300130, China*
[3]*Department of Chemical & Biological Engineering, University of British Columbia, Vancouver, Canada V6T 1Z3*

Correspondence should be addressed to Fei Wang; wangfei@hebut.edu.cn

Received 27 May 2020; Revised 21 June 2020; Accepted 30 June 2020; Published 18 July 2020

Academic Editor: Hao Li

The unique structure of two-dimensional molybdenum disulfide (MoS_2) with rich active sites makes it a promising catalyst, whereas it also brings structural instability. Surfactant-assisted synthesis of MoS_2 can be regarded as a simple way to regulate the microstructure. In this work, the surfactant additives were adopted to optimize the microstructure of MoS_2/sepiolite nanocomposite, and the effects of surfactants type and concentration were investigated. For the sample prepared with 1 mol/L sodium dodecyl benzene sulfonate (SDBS), it exhibits the highest intensity for the peak of MoS_2 at 14.2°, highly dispersed MoS_2 nanosheet on the sepiolite, the lowest absorption intensity of Rhodamine B (RhB) at 553 nm of the wavelength, and the highest photocatalytic activity which is 2.5 times and 4.2 times higher than those prepared with 1 mol/L hexadecyl trimethyl ammonium bromide (CTAB) and 1 mol/L polyvinyl pyrrolidone (PVP) after a 150-minute irradiation, respectively. The above results suggest SDBS is the optimal surfactant to optimize the microstructure of MoS_2/sepiolite nanocomposite. This work could provide new insights into the fabrication of high-quality MoS_2-based nanocomposite.

1. Introduction

As a typical two-dimensional (2D) semiconducting material, MoS_2 with a typical layered structure is formed by stacking of planes. Each plane consists of covalently bonded S-Mo-S atoms in close-packed hexagonal structure, and adjacent planes are held together by van der Waals interactions. MoS_2 has gradually aroused particular interest and enormous attention due to its unique structure which endows MoS_2 with excellent properties for various applications, including photocatalysts [1–3], electrocatalysts [4], supercapacitors [5], sensors [6], and lubricants [7]. However, the high specific surface energy makes it easy agglomeration which results in the decrease of active sites and edges [8]. In order to combat these drawbacks, researchers put their effort to increase the dispersion as well as reduce the layer numbers of MoS_2 nanosheets through different strategies, such as adopting a carrier [9] and taking atomic layer deposition [10]. Nevertheless, the high cost and complex method of preparation restrict them to broad application. In fact, the surfactant-assisted synthesis of MoS_2 has the advantages of low cost, easy operation, and excellent performance, and some surfactants are utilized to optimize MoS_2-based nanocomposite [11–15]. Sepiolite is a typical clay mineral with the features of environment-friendly and low cost, which makes it a good carrier for catalyst because the large surface specific area and excellent adsorption are benefit for the high catalytic performance [16–19]. However, surfactant (cationic, anionic, and non-ionic surfactant) with different charges will affect both catalyst and carrier, due to the surface charge of sepiolite [20, 21]. To date, only few researches have focused on the influences of surfactant on MoS_2 supported by mineral carriers.

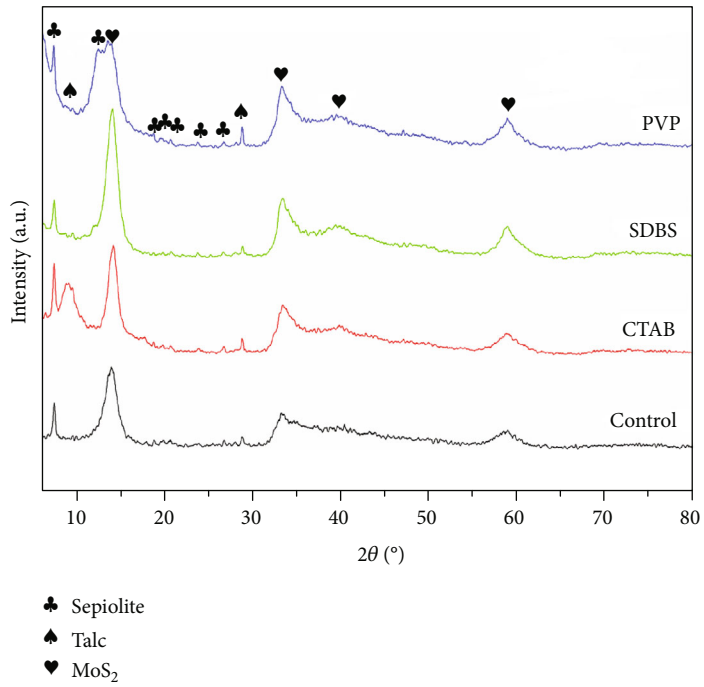

Figure 1: XRD patterns of the samples prepared with different surfactants.

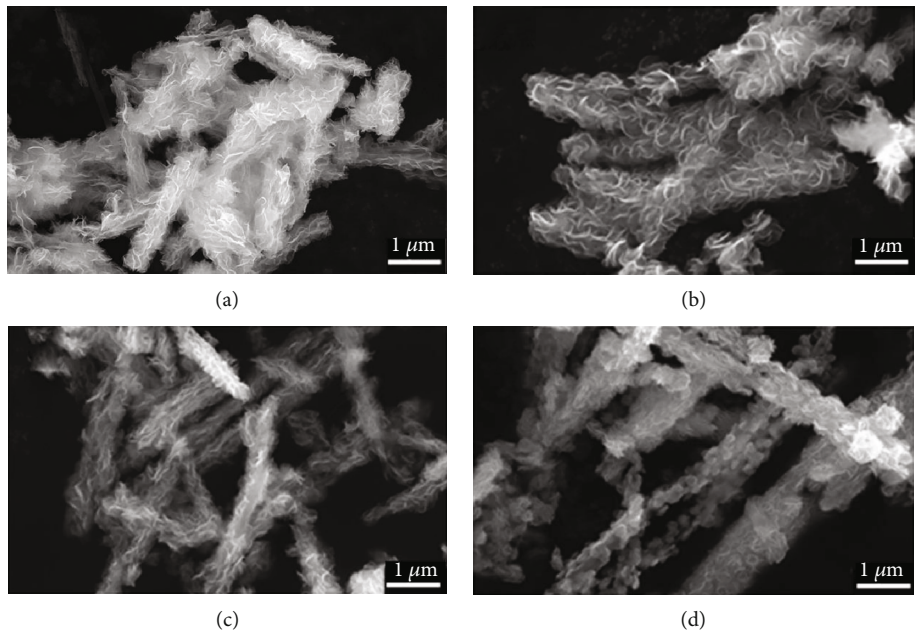

Figure 2: SEM images of the samples prepared with different surfactants. (a) Control; (b) CTAB; (c) SDBS; (d) PVP.

In the previous study, we have found the excellent performance of composites *via*adopting minerals [22–24]. Subsequently, we succeeded in fabricating natural SEP bulks into nano-sized fibers using high-speed airflow techniques [25] and utilized them to achieve the agglomeration decrease of catalysts [26]. Moreover, we also have prepared MoS_2/sepiolite nanocomposite via a microwave hydrothermal method [27]. In this study, the surfactant additives were used to optimize the microstructure of MoS_2/sepiolite nanocomposite, and the effects of surfactants type and concentration were also investigated. This work is believed to offer a new strategy for preparing high-quality MoS_2-based catalyst.

2. Experimental

2.1. Materials. The sepiolite was purchased from Hebei Province, China. All chemical reagents were purchased from Tianjin Damao Chemical Co., Ltd., without further purified.

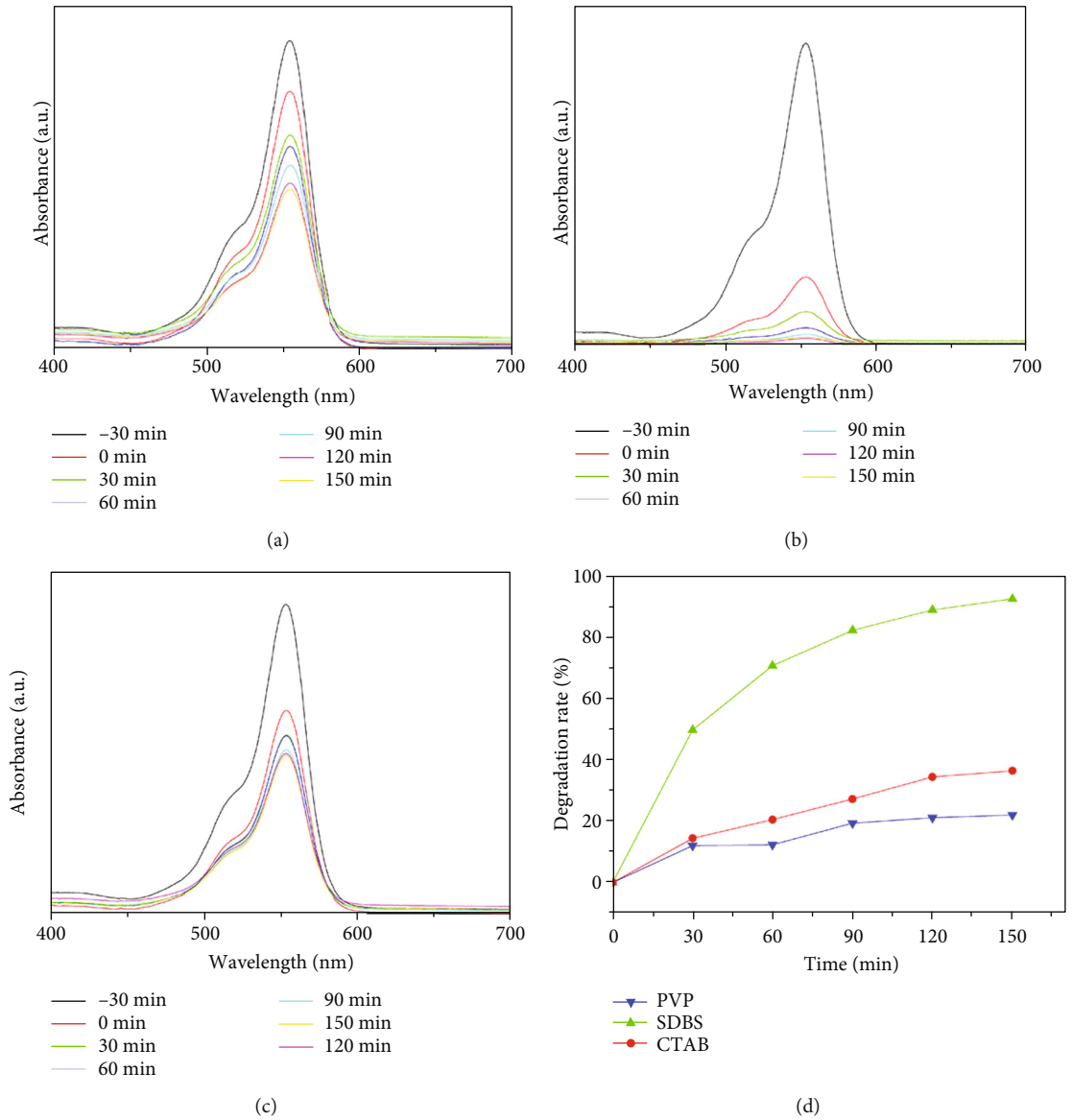

Figure 3: Ultraviolet visible absorption spectra and photocatalysis performance of the samples prepared with different surfactants: (a) CTAB; (b) SDBS; (c) PVP; (d) photocatalytic performance for RhB degradation.

2.2. Sample Preparation. The samples were fabricated by a surfactant-assisted hydrothermal method, and the experimental procedures are similar to reference [27]. In brief, 2 mmol of $(NH_4)_6Mo_7O_{24}{\cdot}4H_2O$, 30 mmol of CH_4N_2S, and appropriate dosage of a certain kind of surfactant (CTAB, SDBS and PVP, respectively) with suitable concentration were dissolved in 70 mL of deionized water and stirred for 30 min. Then, 0.6 g of sepiolite nanofiber powders prepared *via* high-speed airflow techniques [25] for the natural SEP bulks were added into the solution and kept stirring for another 0.5 h. Next, the mixture was sonicated for 10 min. After that, 50 mL of the above suspension was transferred to a 100 mL Teflon-lined stainless steel autoclave and kept at 220°C for 3 h under microwave heating. After the samples were cooled down to room temperature, the final products were obtained by filtration, washed several times with deionized water, and dried in the vacuum oven at 80°C for 12 h.

2.3. Characterization and Performance Tests. X-ray powder diffraction (XRD) was performed by a D8 ADVANCE X-ray diffractometer with nickel-filtered ($V = 40$ kV, $I = 40$ mA) Cu Kα radiation as the X-ray source ($\lambda = 1.54$ Å). The morphologies of the as-synthesized samples were observed by SEM (FEI Nano SEM450) under an accelerating voltage of 1.00 kV.

The photocatalytic activity of the as-prepared samples was tested through the photocatalytic degradation of RhB under visible light irradiation. 20 mg of samples were dispersed into 100 mL of RhB solution (20 mg/L), stirring the produced suspension in the dark for 30 min to reach the adsorption/desorption equilibrium. The suspension was subjected to irradiation by a 500 W Xe lamp ($\lambda > 420$ nm) under stirring at ambient conditions. After 30 min, 6 mL of the suspension was taken out and centrifuged to remove the photocatalysts. The filtrates were analyzed through recording the

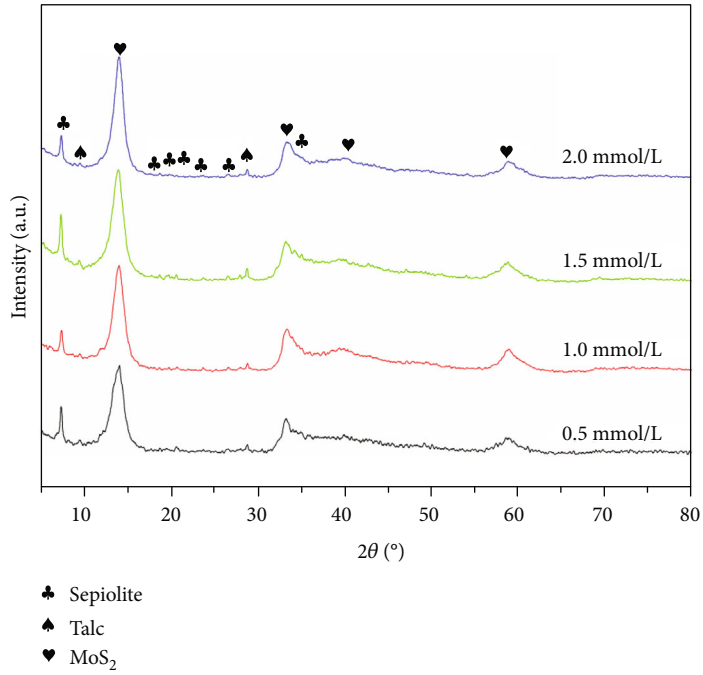

Figure 4: XRD patterns of the samples prepared with different concentration of SDBS.

UV-Vis spectra by a Shimadzu UV-1800 spectrophotometer. The calculated method of photodegradation efficiency was shown in equation (1) where D represents the photodegradation efficiency of catalyst, A_0 represents the absorbance value at the beginning of illumination, and A_t represents the absorbance value at a certain time t of illumination.

$$D(\%) = (A_0 - A_t)/A_0. \quad (1)$$

3. Results and Discussion

Figure 1 shows the XRD patterns of the samples prepared with different surfactants. The two main phases are sepiolite and 2H-MoS_2 which are unchanged, indicating the structure of nanocomposite kept stable after adding surfactant [28, 29]. Compared with the control sample, surfactant-assisted synthesis of nanocomposite exhibits sharper peaks of MoS_2 (101) and (110) facets at 33.5° and 58.3°, respectively, which suggests the better crystallinity of MoS_2. Meanwhile, the sample prepared with SDBS shows the highest intensity for the peak of MoS_2 (002) facet at 14.2°, suggesting the increased content of MoS_2 [30]. Besides, the sample prepared by the similar process coupled with PVP or CTAB has almost no influence on the MoS_2 phase in nanocomposite.

SEM images directly show the morphology of sample prepared with different surfactants (Figure 2). Sample prepared with PVP suffers from serious agglomeration where MoS_2 nanosheets transferred to a microsphere morphology contrast to the control sample (Figures 2(a) and 2(d)), while MoS_2 in nanocomposite remains the good dispersion when CTAB or SDBS are added (Figures 2(b) and 2(c)). The sample morphology suggests that PVP is not suitable to optimize the MoS_2 supported by sepiolite.

To further identify the optimal surfactant, photocatalytic degradation of RhB is adopted as a probe reaction. As shown in Figure 3, the absorbance of RhB for all samples decreased at the maximum absorption wavelength along with the increase of lighting time. However, the sample prepared with SDBS has the maximum descent, compared with those used CTAB and PVP after a 150-minute irradiation (Figures 3(a)–3(c)). Moreover, the degradation efficiency of RhB for the sample prepared with SDBS reaches about 93% after irradiation of 150 minutes (Figure 3(d)), which is much higher than those prepared with CTAB (37%) and PVP (22%). Combined with the results of XRD, SEM, and photocatalysis performance, SDBS can be identified as the optimal surfactant.

The most suitable concentration of the SDBS is studied subsequently. As shown in Figure 4, the samples prepared with 1 mol/L and 1.5 mol/L SDBS show the sharper peaks of MoS_2 (101) and (110) facets at 33.5° and 58.3°, respectively, which indicates the appropriate concentration of SDBS can increased crystallinity of MoS_2 in nanocomposite while sample prepared with too high (2 mol/L) or low (0.5 mol/L) concentration of SDBS is unsuitable.

Figure 5 shows the morphology of the samples prepared with different concentration of SDBS. It can be seen that MoS_2 in nanocomposite remains the architecture of nanosheet and disperses on the sepiolite surface, but the MoS_2 on the surface of sepiolite disperses sparsely when the concentration is 0.5 mol/L (Figure 5(a)). When the concentration comes up to 1.5 mol/L and 2 mol/L, a few parts of MoS_2 suffer from slight agglomeration (Figures 5(c) and 5(d)). When the concentration is 1 mol/L, the MoS_2 nanosheets are uniformly dispersed on the sepiolite surface with the high density and no obvious agglomeration (Figure 5(b)). Consequently, the concentration of SDBS has

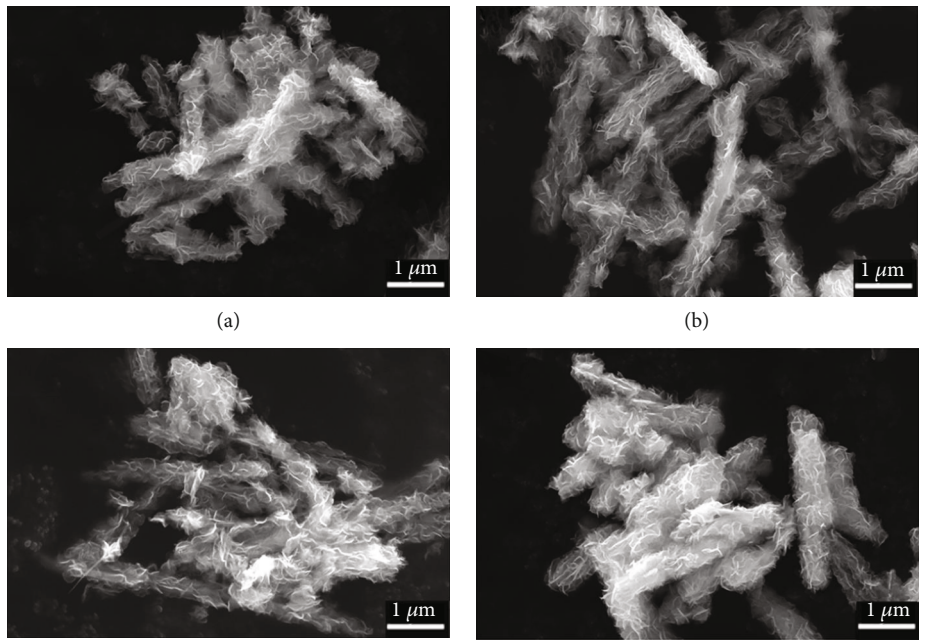

Figure 5: SEM images of the samples prepared with different concentration of SDBS. (a) 0.5 mmol/L; (b) 1.0 mmol/L; (c) 1.5 mmol/L; (d) 2.0 mmol/L.

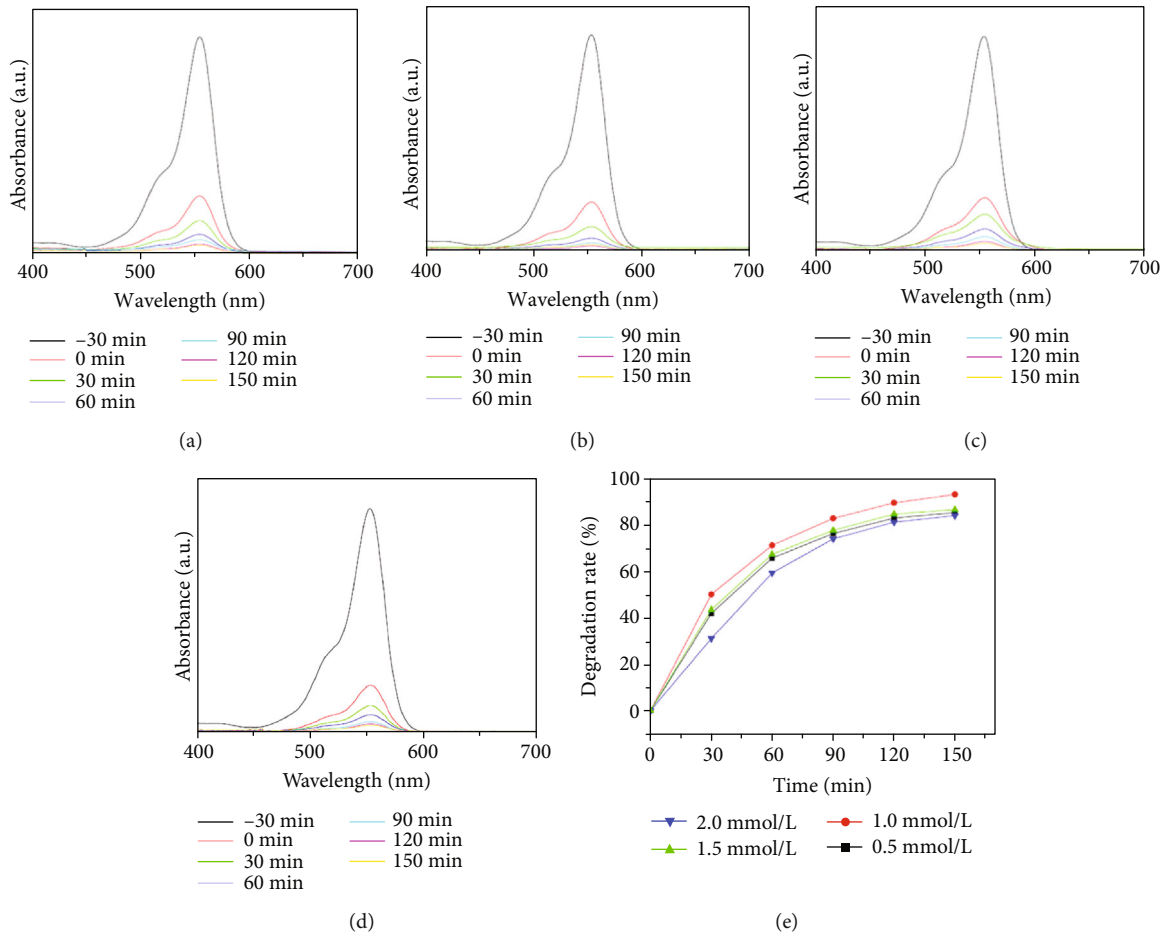

Figure 6: Ultraviolet visible absorption spectra and photocatalysis performance of the sample prepared with different concentration of SDBS. (a) 0.5 mmol/L; (b) 1.0 mmol/L; (c) 1.5 mmol/L; (d) 2.0 mmol/L; (e) photocatalytic performance for RhB degradation.

obvious influence on the dispersion of MoS_2 in the nanocomposite.

The ultraviolet visible absorption spectra and photocatalytic performance of the samples prepared with different concentration of SDBS are also studied to find the optimal condition (Figure 6). The sample prepared with 1 mol/L SDBS has the maximum descent for the absorbance of RhB compared with those used other concentrations (Figures 6(a)–6(d)). In addition, photocatalytic activity of samples toward RhB degradation can be as an important evidence to obtain the optimal concentration of SDBS, and the RhB degradation efficiency of the sample prepared with 1 mol/L SDBS is the highest (Figure 6(e)). Thus, the optimal concentration of SDBS can be identified as 1 mol/L.

4. Conclusions

In summary, MoS_2/sepiolite nanocomposite was optimized via a surfactant-assisted hydrothermal method, and the influence of surfactants type and concentration was also studied. The results show that the photocatalysis activity of the nanocomposite prepared with 1 mol/L SDBS as the optimal condition toward RhB degradation reaches about 93%, which is extremely higher than those used CTAB and PVP with the same concentration. SEM images directly show the microsphere MoS_2 suffering from serious agglomeration when using PVP. Meanwhile, the increased content of $MoS_2$is exhibited with the present of SDBS. Among the sample prepared with different concentrations of SDBS, 1 mol/L SDBS as the optimal concentration makes the best crystallinity of MoS_2 in nanocomposite. This work provides a new perspective for regulating the microstructure of MoS_2-based catalyst.

Data Availability

The manuscript contains all of the data.

Conflicts of Interest

There is no conflict interest to declare.

Authors' Contributions

Li Cui and Ming Hao contributed equally to this work.

Acknowledgments

This work was financially supported by the National Natural Science Foundation of China (No. 51874115), Introduced Overseas Scholars Program of Hebei Province, China (No. C201808), Enterprise Science and Technology Commissioner Project of Tianjin City, China (No. 19JCTPJC56100), and Excellent Young Scientist Foundation of Hebei Province, China (No. E2018202241).

References

[1] Z. Wu, X. He, Y. Xue et al., "Cyclodextrins grafted MoS_2/g-C_3N_4 as high-performance photocatalysts for the removal of glyphosate and Cr (VI) from simulated agricultural runoff," *Chemical Engineering Journal*, vol. 399, p. 125747, 2020.

[2] B. Chen, Y. Meng, J. Sha, C. Zhong, W. Hu, and N. Zhao, "Preparation of MoS_2/TiO_2 based nanocomposites for photocatalysis and rechargeable batteries: progress, challenges, and perspective," *Nanoscale*, vol. 10, no. 1, pp. 34–68, 2018.

[3] H. He, J. Lin, W. Fu et al., "MoS_2/TiO_2 edge-on heterostructure for efficient photocatalytic hydrogen evolution," *Advanced Energy Materials*, vol. 6, no. 14, p. 1600464, 2016.

[4] Y. Yang, K. Zhang, H. Lin et al., "MoS_2–Ni_3S_2 heteronanorods as efficient and stable bifunctional electrocatalysts for overall water splitting," *ACS Catalysis*, vol. 7, no. 4, pp. 2357–2366, 2017.

[5] H. Tang, J. Wang, H. Yin, H. Zhao, D. Wang, and Z. Tang, "Growth of polypyrrole ultrathin films on MoS_2 monolayers as high-performance supercapacitor electrodes," *Advanced Materials*, vol. 27, no. 6, pp. 1117–1123, 2015.

[6] S. Y. Park, J. E. Lee, Y. H. Kim et al., "Room temperature humidity sensors based on rGO/MoS_2 hybrid composites synthesized by hydrothermal method," *Sensors and Actuators B-chemical*, vol. 258, pp. 775–782, 2018.

[7] H. Xie, B. Jiang, J. He, X. Xia, and F. Pan, "Lubrication performance of MoS_2 and SiO_2 nanoparticles as lubricant additives in magnesium alloy-steel contacts," *Tribology International*, vol. 93, pp. 63–70, 2016.

[8] J. Zhou, M. Guo, L. Wang et al., "1T-MoS_2 nanosheets confined among TiO_2 nanotube arrays for high performance supercapacitor," *Chemical Engineering Journal*, vol. 366, pp. 163–171, 2019.

[9] D. Sun, D. Ye, P. Liu et al., "MoS_2/graphene nanosheets from commercial bulky MoS_2 and graphite as anode materials for high rate sodium-ion batteries," *Advanced Energy Materials*, vol. 8, no. 10, p. 1702383, 2018.

[10] J. Yang and L. Liu, "Trickle flow aided atomic layer deposition (ALD) strategy for ultrathin molybdenum disulfide (MoS_2) synthesis," *ACS Applied Materials & Interfaces*, vol. 11, no. 39, pp. 36270–36277, 2019.

[11] M. Li, D. Wang, J. Li et al., "Surfactant-assisted hydrothermally synthesized MoS_2 samples with controllable morphologies and structures for anthracene hydrogenation," *Chinese Journal of Catalysis*, vol. 38, no. 3, pp. 597–606, 2017.

[12] Y. Zhang, W. Zeng, and Y. Li, "The hydrothermal synthesis of 3D hierarchical porous MoS_2 microspheres assembled by nanosheets with excellent gas sensing properties," *Journal of Alloys and Compounds*, vol. 749, no. 15, pp. 355–362, 2018.

[13] S. Kumari, R. Gusain, N. Kumar, and O. P. Khatri, "PEG-mediated hydrothermal synthesis of hierarchical microspheres of MoS_2 nanosheets and their potential for lubrication application," *Journal of Industrial and Engineering Chemistry*, vol. 42, pp. 87–94, 2016.

[14] X. Zeng and W. Qin, "Synthesis of MoS_2 nanoparticles using MoO_3 nanobelts as precursor via a PVP-assisted hydrothermal method," *Materials Letters*, vol. 182, pp. 347–350, 2016.

[15] A. Trenczekzajac, J. Banas, and M. Radecka, "Photoactive TiO_2/MoS_2 electrode with prolonged stability," *International Journal of Hydrogen Energy*, vol. 43, no. 14, pp. 6824–6837, 2018.

[16] H. Li, W. Chai, and G. Henkelman, "Selectivity for ethanol partial oxidation: the unique chemistry of single-atom alloy catalysts on Au, Ag, and Cu (111)," *Journal of Materials Chemistry A*, vol. 7, no. 41, pp. 23868–23877, 2019.

[17] Y. Piao, Q. Jiang, H. Li et al., "Identify Zr promotion effects in atomic scale for Co-based catalysts in Fischer-Tropsch synthesis," *ACS Catalysis*, vol. 10, pp. 7894–7906, 2020.

[18] X. Hu, Z. Sun, J. Song, G. Zhang, C. Li, and S. Zheng, "Synthesis of novel ternary heterogeneous BiOCl/TiO_2/sepiolite composite with enhanced visible-light-induced photocatalytic activity towards tetracycline," *Journal of Colloid and Interface Science*, vol. 533, pp. 238–250, 2019.

[19] H. Li, S. Guo, K. Shin, M. S. Wong, and G. Henkelman, "Design of a Pd-Au nitrite reduction catalyst by identifying and optimizing active ensembles," *ACS Catalysis*, vol. 9, no. 9, pp. 7957–7966, 2019.

[20] F. Wang, M. Hao, J. Liang et al., "A facile fabrication of sepiolite mineral nanofibers with excellent adsorption performance for Cd^{2+} ions," *RSC Advances*, vol. 9, no. 69, pp. 40184–40189, 2019.

[21] J. A. Carmona, P. Ramírez, L. A. Trujillo-Cayado, A. Caro, and J. Muñoz, "Rheological and microstructural properties of sepiolite gels. Influence of the addition of ionic surfactants," *Journal of Industrial and Engineering Chemistry*, vol. 59, pp. 1–7, 2018.

[22] F. Wang, P. Gao, J. Liang et al., "A novel and simple microwave hydrothermal method for preparation of $CoAl_2O_4$/sepiolite nanofibers composite," *Ceramics International*, vol. 45, no. 18, pp. 24923–24926, 2019.

[23] Q. Tang, F. Wang, X. Liu et al., "Surface modified palygorskite nanofibers and their applications as reinforcement phase in cis-polybutadiene rubber nanocomposites," *Applied Clay Science*, vol. 132-133, pp. 175–181, 2016.

[24] F. Wang, Z. Xie, J. Liang et al., "Tourmaline-modified FeMn-TiO_x catalysts for improved low-temperature NH_3-SCR performance," *Environmental Science & Technology*, vol. 53, no. 12, pp. 6989–6996, 2019.

[25] J. Liang, F. Wang, Q. Tang et al., "A method of preparing mineral nanofiber," 2009, CN 200910070297.8.

[26] T. Zhang, F. Wang, J. Liang et al., "A novel and facile impregnation-combustion fabrication of spherical $CoAl_2O_4$ supported on sepiolite nanofibers," *Ceramics International*, vol. 44, no. 16, pp. 19543–19546, 2018.

[27] F. Wang, M. Zhu, J. Liang et al., "Preparation method of MoS_2-sepiolite nanofiber composite," 2018, CN 201810359072.3.

[28] Y. Zhang, L. Wang, F. Wang, J. Liang, S. Ran, and J. Sun, "Phase transformation and morphology evolution of sepiolite fibers during thermal treatment," *Applied Clay Science*, vol. 143, pp. 205–211, 2017.

[29] S. Karunakaran, S. Pandit, B. Basu, and M. de, "Simultaneous exfoliation and functionalization of 2H-MoS_2 by thiolated surfactants: applications in enhanced antibacterial activity," *Journal of the American Chemical Society*, vol. 140, no. 39, pp. 12634–12644, 2018.

[30] D. Wang, Y. Xu, F. Sun, Q. Zhang, P. Wang, and X. Wang, "Enhanced photocatalytic activity of TiO_2 under sunlight by MoS_2 nanodots modification," *Applied Surface Science*, vol. 377, pp. 221–227, 2016.